Int. J. Solids Structures Vol. 27, No. 9, pp. 1139–1153, 1991
Printed in Great Britain.

0020–7683/91 $3.00 + .00

MIXED MODE FRACTURE OF CONCRETE

PIETRO BOCCA, ALBERTO CARPINTERI and SILVIO VALENTE
Politecnico di Torino, Department of Structural Engineering, 10129 Torino, Italy

(*Received* 18 *July* 1989; *in revised form* 15 *March* 1990)

Abstract—Strain-softening and strain-localization in cementitious and ceramic materials can be described by using a cohesive crack model, with closing forces at the crack tip, which represent plasticity, inclusion interlocking, fibre bridging and any kind of non-linear behaviour. In the present paper, the cohesive crack model is extended to mixed mode propagation and an experimental confirmation is provided by testing four-point shear specimens of concrete. A constant crack mouth sliding displacement rate is imposed, so that is is possible to control and detect the snap-back load vs deflection branches. The behaviour of the larger specimens is found to be the brittler. On the other hand, the brittleness in the numerical simulations is controlled through the crack length, which is certainly a monotonic increasing function during the irreversible fracture process. The experimental load vs deflection diagrams as well as the experimental fracture trajectories are captured satisfactorily by the numerical model. The mixed mode fracture energy results tend to be of the same order of magnitude as the Mode I fracture energy $\mathcal{G}_F$, each elementary crack growth step being produced by an opening mechanism along the curvilinear trajectory. This is particularly true for the larger specimens, where energy dissipation due to friction and interlocking is negligible if compared with the energy dissipated by separation.

1. INTRODUCTION

In cementitious and ceramic materials strain-softening prevails over strain-hardening and strain-localization can be taken into account using a cohesive crack idealization. According to the cohesive crack model, the non-linear structure and crack behaviour can be described by means of cohesive closing forces in the process zone, which represent plastic flow, aggregate interlocking, fibre bridging, etc.

The cohesive crack model was originally proposed by Barenblatt (1959) and, independently, by Dugdale (1960). Later, it was reconsidered by Bilby *et al.* (1963), Willis (1967) and Rice (1968). More recently, the cohesive crack model was reproposed, with some modifications, by Wnuk (1974)—the Final Stretch Model—and by Hillerborg *et al.* (1976)—the Fictitious Crack Model. The latter was applied mostly to concrete-like materials and numerically implemented in a finite element program.

In the present paper, the cohesive crack model is extended to mixed mode propagation, when the crack is loaded by opening and sliding forces and it turns aside at each step. For Mode I (Carpinteri, 1989a, b; Carpinteri and Colombo, 1989), and for mixed mode, the shape of the structural response changes substantially by varying size-scale and keeping the geometrical shape of the structure unchanged. For size-scales larger than a threshold value, a snap-back instability appears, when the plastic zone is still absent and the slow crack growth has not yet occurred. Asymptotically, the snap-back instability coincides with the LEFM instability and the snap-back load can be provided by the simple LEFM condition $K_I = K_{IC}$, in Mode I, or by the Maximum Circumferential Stress Criterion (Erdogan and Sih, 1963): $F(K_I, K_{II}) = K_{IC}$, in mixed mode.

An experimental program consisting of 27 four-point shear specimens of concrete was carried out, with the sizes scaled in the proportion 1 : 2 : 4. The loading machine imposed a constant crack mouth sliding displacement rate, so that it was possible to control and detect the snap-back branches. On the other hand, the snap-back branches can be captured numerically only if the loading process is controlled by a monotonically increasing function of the crack length. An example of such a function is provided by the "indirect displacement control scheme" (Rots and de Borst, 1987). This technique uses a displacement norm as controlling parameter. On the other hand, as a monotonically increasing function of the crack length, it is possible to use the crack length itself, in Mode I (Carpinteri, 1984; Carpinteri and Fanelli, 1987) as well as in mixed mode (Carpinteri and Valente, 1988;

Carpinteri *et al.*, 1989). Such a technique, called the "crack length control scheme", will be proposed in the present paper.

Finite element crack propagation requires a continuous modification of the mesh. Whereas for Mode I (Carpinteri, 1989a, b), only node untying can be applied to simulate crack growth, for mixed mode a topological variation is performed at each step of the interelement crack propagation, following an automatic procedure which is similar to that proposed by Wawrzynek and Ingraffea (1987).

2. EXPERIMENTAL PROGRAM

Twenty-seven four-point shear specimens of concrete were tested. The quantity of Portland cement was 350 kg m^{-3}, while the water/cement ratio was taken to be 0.5. The maximum diameter of the alluvial aggregates was $D_{max} = 10$ mm. The average compressive strength obtained from six cubic specimens with 16 cm sides was 33.7 MPa. The specimens were cured for 90 days at 20°C and 65% relative humidity.

The geometrical features of the specimens were as follows (Figs 1 and 2):

depth $b = 5, 10, 20$ cm;
span $l = 4b$;
thickness $t = 10$ cm;
crack depth $a = 0.2b$;
c/b ratio $= 0.4, 0.8, 1.2$.

The specimen geometry, support configuration and mechanical properties are provided in Table 1.

The testing apparatus is shown in Fig. 3. The MTS machine (max. load $= 10^5$ N) imposed a constant crack mouth sliding displacement rate equal to 2.5×10^{-8} m s^{-1} through the displacement transducer (Hottinger Baldwin DD1). A similar transducer recorded the load vs crack mouth opening displacement diagram, together with the load vs loading point deflection diagram for the support closest to the center.

In addition, four specimens of size $10 \times 10 \times 80$ cm, were tested in three-point bending according to the RILEM Recommendation (1985): the Mode I fracture energy was found to be $\mathcal{G}_F \approx 100$ N m^{-1}.

3. NUMERICAL COHESIVE CRACK MODEL

The principle of virtual work can be used as the integral statement to formulate the elastic-softening problem in terms of the finite element approximation:

$$\int_V d\boldsymbol{\varepsilon}^T \boldsymbol{\sigma}\, dV = \int_V d\mathbf{u}^T \mathbf{F}\, dV + \int_S d\mathbf{u}^T \mathbf{p}\, dS, \tag{1}$$

where $\boldsymbol{\sigma}^T = [\sigma_x, \sigma_y, \sigma_z, \tau_{xy}, \tau_{yz}, \tau_{xz}]$ is the stress vector, $d\boldsymbol{\varepsilon}^T$ is the vector of incremental virtual

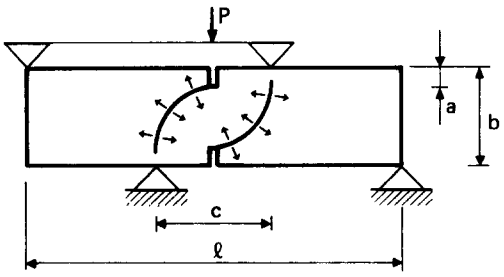

Fig. 1. Four-point shear specimen.

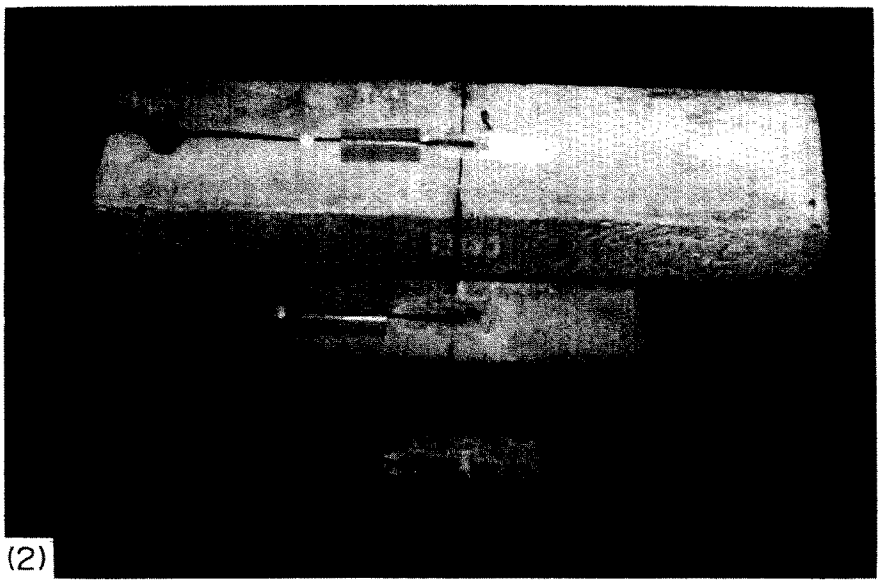

Fig. 2. Different specimen sizes selected for the experimental investigation.

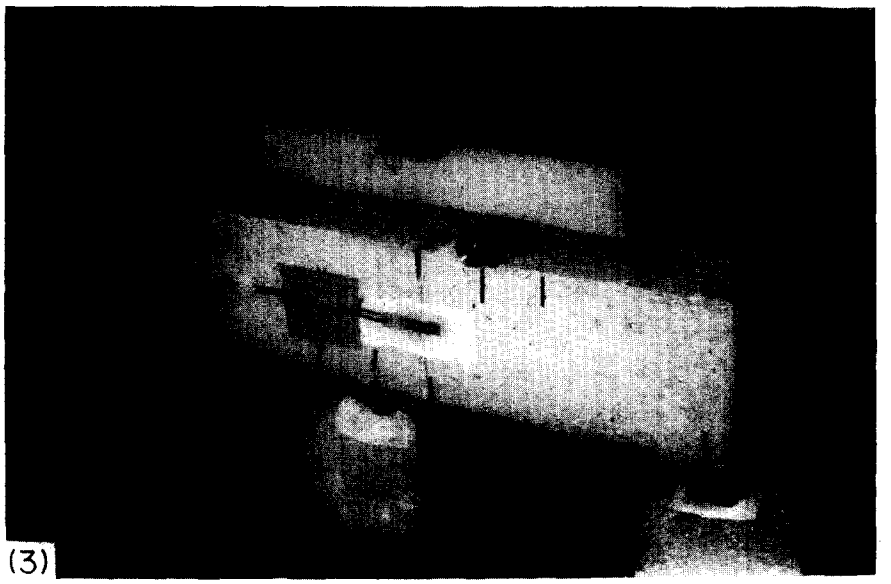

Fig. 3. Testing apparatus.

Table 1. Specimen geometry, support configuration and mechanical properties

Specimen size	Number of specimens	b	l	t	a	c/b	Maximum load average, P_{max} (dN)
		($m \times 10^{-2}$)					
A	3	5	20	10	1	0.4	1190
	3	5	20	10	1	0.8	1222
	3	5	20	10	1	1.2	1370
B	3	10	40	10	2	0.4	2027
	3	10	40	10	2	0.8	1980
	3	10	40	10	2	1.2	1535
C	3	20	80	10	4	0.4	3493
	3	20	80	10	4	0.8	3446
	3	20	80	10	4	1.2	3700
$R_c = 33.7$ MPa $E = 27{,}000$ MPa		$\sigma_u \approx 2$ MPa $\mathcal{G}_F \approx 100\,\mathrm{N\,m^{-1}}$					

strain, $\mathbf{F}^T = [F_x, F_y, F_z]$ is the vector of body forces acting per unit volume, $\mathbf{du}^T = [du, dv, dw]$ is the vector of incremental virtual displacement and $\mathbf{p}^T = [p_x, p_y, p_z]$ is the vector of tractions acting per unit area of external surface S. Equation (1) is the weak form of the equilibrium equations and is valid for linear as well as for non-linear stress–strain constitutive laws.

According to the cohesive crack model, the process zone near the crack tip can be represented by means of closing tractions $\mathbf{p}_c$ acting on both the crack faces. Therefore, the last term in eqn (1) can be decomposed as follows (Fig. 1):

$$\int_S \mathbf{du}^T \mathbf{p}\, dS = \int_{S_c} \mathbf{du}^T \mathbf{p}_c\, dS + \int_{S-S_c} \mathbf{du}^T \mathbf{p}\, dS, \tag{2}$$

where S_c is the process zone, i.e., the crack surface where the cohesive forces are active. A local reference system, with Z-axes oriented as the outward normal to the positive side of the crack surface, is assumed. $\mathbf{N}$ is the transformation matrix from the global to the local reference system, varying point by point on the crack surface. Assuming a linear softening constitutive law, the traction versus displacement relationship can therefore be written (Fig. 4):

$$\mathbf{p}_c = \mathbf{p}_u + \mathbf{N}^T \mathbf{L} \mathbf{N} (\mathbf{u}^+ - \mathbf{u}^-), \tag{3}$$

where $\mathbf{p}_u$ is the ultimate tensile strength in vectorial form, $\mathbf{N}$ is the transformation matrix from the global to the local reference system, varying point by point on the crack surface,

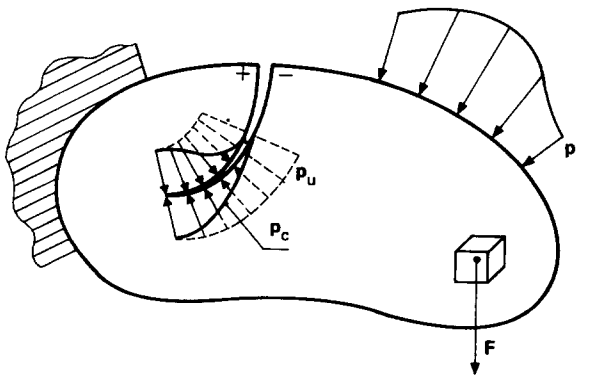

Fig. 4. Mixed mode cohesive crack propagation.

L is the cohesive constitutive matrix in a local Cartesian system, the index + refers to the positive side of the crack, while the index − refers to the negative one.

From equilibrium considerations across the crack surface, it is possible to write:

$$\mathbf{p}_c^+ = -\mathbf{p}_c^-, \quad \mathbf{p}_u^+ = -\mathbf{p}_u^-, \quad S_c^+ = S_c^- = S_c/2. \tag{4}$$

The first term in the right-hand side of eqn (2) can be written:

$$\int_{S_c} \mathrm{d}\mathbf{u}^{\mathrm{T}}\mathbf{p}_c \,\mathrm{d}S = \int_{S_c^+} \mathrm{d}\mathbf{u}^{+\mathrm{T}}\mathbf{p}_u^+ \,\mathrm{d}S + \int_{S_c^-} \mathrm{d}\mathbf{u}^{-\mathrm{T}}\mathbf{p}_u^- \,\mathrm{d}S + \int_{S_c^+} \mathrm{d}\mathbf{u}^{+\mathrm{T}}\mathbf{N}^{\mathrm{T}}\mathbf{L}\mathbf{N}(\mathbf{u}^+ - \mathbf{u}^-)\,\mathrm{d}S - \int_{S_c^-} \mathrm{d}\mathbf{u}^{-\mathrm{T}}\mathbf{N}^{\mathrm{T}}\mathbf{L}\mathbf{N}(\mathbf{u}^+ - \mathbf{u}^-)\,\mathrm{d}S. \tag{5}$$

The last two terms in eqn (5) can be represented as follows:

$$\int_{S_c/2} \begin{Bmatrix} \mathrm{d}\mathbf{u}^+ \\ \mathrm{d}\mathbf{u}^- \end{Bmatrix}^{\mathrm{T}} \begin{bmatrix} \mathbf{N}^{\mathrm{T}} & \mathbf{0} \\ \mathbf{0} & \mathbf{N}^{\mathrm{T}} \end{bmatrix} \begin{bmatrix} \mathbf{L} & -\mathbf{L} \\ -\mathbf{L} & \mathbf{L} \end{bmatrix} \begin{bmatrix} \mathbf{N} & \mathbf{0} \\ \mathbf{0} & \mathbf{N} \end{bmatrix} \begin{Bmatrix} \mathbf{u}^+ \\ \mathbf{u}^- \end{Bmatrix} \mathrm{d}S. \tag{6}$$

The principle of virtual work, eqn (1), can be developed according to eqns (2), (5) and (6):

$$\int_V \mathrm{d}\boldsymbol{\varepsilon}^{\mathrm{T}}\boldsymbol{\sigma}\,\mathrm{d}V = \int_V \mathrm{d}\mathbf{u}^{\mathrm{T}}\mathbf{F}\,\mathrm{d}V + \int_{S-S_c} \mathrm{d}\mathbf{u}^{\mathrm{T}}\mathbf{p}\,\mathrm{d}S + \int_{S_c^+} \mathrm{d}\mathbf{u}^{+\mathrm{T}}\mathbf{p}_u^+\,\mathrm{d}S + \int_{S_c^-} \mathrm{d}\mathbf{u}^{-\mathrm{T}}\mathbf{p}_u^-\,\mathrm{d}S + \int_{S_c/2} \begin{Bmatrix} \mathrm{d}\mathbf{u}^+ \\ \mathrm{d}\mathbf{u}^- \end{Bmatrix}^{\mathrm{T}} \begin{bmatrix} \mathbf{N}^{\mathrm{T}} & \mathbf{0} \\ \mathbf{0} & \mathbf{N}^{\mathrm{T}} \end{bmatrix} \begin{bmatrix} \mathbf{L} & -\mathbf{L} \\ -\mathbf{L} & \mathbf{L} \end{bmatrix} \begin{bmatrix} \mathbf{N} & \mathbf{0} \\ \mathbf{0} & \mathbf{N} \end{bmatrix} \begin{Bmatrix} \mathbf{u}^+ \\ \mathbf{u}^- \end{Bmatrix} \mathrm{d}S. \tag{7}$$

Subdividing the domain in a finite number of elements and expressing the internal displacements by means of locally based shape functions **H**, it is possible to write:

$$\mathbf{u}(x, y, z) = \mathbf{H}(x, y, z)\mathbf{u}. \tag{8}$$

From the derivation of eqn (8), the strain versus displacement relationship can be obtained:

$$\boldsymbol{\varepsilon} = \mathbf{B}\mathbf{u}. \tag{9}$$

Selecting an appropriate constitutive law for the uncracked zone, the stress versus strain relationship appears as follows:

$$\boldsymbol{\sigma} = \mathbf{D}(\boldsymbol{\varepsilon} - \boldsymbol{\varepsilon}_0) + \boldsymbol{\sigma}_0. \tag{10}$$

Substituting eqns (8), (9) and (10) in eqn (7), and indicating by "e" the generic element, it is possible to write:

$$\mathrm{d}\mathbf{u}^{\mathrm{T}}\left(\sum_e \int_V \mathbf{B}^{\mathrm{T}}\mathbf{D}\mathbf{B}\,\mathrm{d}V\right)\mathbf{u} - \begin{Bmatrix} \mathrm{d}\mathbf{u}^+ \\ \mathrm{d}\mathbf{u}^- \end{Bmatrix}^{\mathrm{T}} \left(\sum_e \int_{S_c/2} \begin{bmatrix} \mathbf{H}^{\mathrm{T}}\mathbf{N}^{\mathrm{T}} & \mathbf{0} \\ \mathbf{0} & \mathbf{H}^{\mathrm{T}}\mathbf{N}^{\mathrm{T}} \end{bmatrix} \begin{bmatrix} \mathbf{L} & -\mathbf{L} \\ -\mathbf{L} & \mathbf{L} \end{bmatrix} \begin{bmatrix} \mathbf{N}\mathbf{H} & \mathbf{0} \\ \mathbf{0} & \mathbf{N}\mathbf{H} \end{bmatrix} \mathrm{d}S\right) \times \begin{Bmatrix} \mathbf{u}^+ \\ \mathbf{u}^- \end{Bmatrix} = \mathrm{d}\mathbf{u}^{\mathrm{T}}\left(\sum_e \int_V (\mathbf{H}^{\mathrm{T}}\mathbf{F} - \mathbf{B}^{\mathrm{T}}\boldsymbol{\sigma}_0 + \mathbf{B}^{\mathrm{T}}\mathbf{D}\boldsymbol{\varepsilon}_0)\,\mathrm{d}V\right) + \mathrm{d}\mathbf{u}^{\mathrm{T}}\left(\sum_e \int_{S-S_c} \mathbf{H}^{\mathrm{T}}\mathbf{p}\,\mathrm{d}S\right) + \mathrm{d}\mathbf{u}^{+\mathrm{T}}\left(\sum_e \int_{S_c^+} \mathbf{H}^{\mathrm{T}}\mathbf{p}_u^+\,\mathrm{d}S\right) + \mathrm{d}\mathbf{u}^{-\mathrm{T}}\left(\sum_e \int_{S_c^-} \mathbf{H}^{\mathrm{T}}\mathbf{p}_u^-\,\mathrm{d}S\right). \tag{11}$$

Since:

$$\{\mathbf{u}^+\} \subset \{\mathbf{u}\}, \quad \{\mathbf{u}^-\} \subset \{\mathbf{u}\}, \quad \{\mathbf{du}^+\} \subset \{\mathbf{du}\}, \quad \{\mathbf{du}^-\} \subset \{\mathbf{du}\}, \tag{12}$$

an assemblage procedure can be carried out:

$$(\mathbf{K}-\mathbf{C})\mathbf{u} = \mathbf{F}_v + \mathbf{F}_s + \mathbf{F}_u^+ + \mathbf{F}_u^-, \tag{13}$$

where

$$\begin{aligned} \mathbf{K} &= \text{stiffness matrix,} \\ \mathbf{C} &= \text{softening matrix,} \\ \mathbf{F}_v, \mathbf{F}_s, \mathbf{F}_u^+, \mathbf{F}_u^- &= \text{loading vectors,} \\ (\mathbf{K}-\mathbf{C}) &= \text{effective stiffness matrix.} \end{aligned}$$

Neglecting the tangential cohesive tractions, the constitutive matrix $\mathbf{L}$ becomes:

$$\mathbf{L} = \begin{bmatrix} 0 & 0 & 0 \\ 0 & 0 & 0 \\ 0 & 0 & l_{33} \end{bmatrix}. \tag{14}$$

Only the component of the mutual displacement normal to the crack surface, w (crack opening displacement), is taken into account. The remaining components are disregarded. The scalar quantity l_{33} is assumed as follows:

$$l_{33} = \frac{\sigma_u}{w_c}, \quad \text{for} \quad 0 < w < w_c, \tag{15a}$$

$$l_{33} = 0, \quad \text{for} \quad w \geqslant w_c, \tag{15b}$$

where σ_u is the ultimate tensile strength of the material and w_c is the critical value of the crack opening displacement w. For crack opening displacements greater than the critical value w_c, the interaction forces disappear, and both the crack surfaces are stress-free. During the irreversible fracture process, the crack opening displacement w is found to be a monotonic increasing function of time.

At the first step the cohesive zone is absent, matrix $\mathbf{C}$ vanishes and matrix $\mathbf{K}$ is positive definite. A linear elastic solution can be found, giving the position and orientation of the growing crack. The crack surface S_c starts propagating by a pre-defined length ΔS_c. Such an incremental length is chosen so small that matrix $(\mathbf{K}-\mathbf{C})$ remains positive definite, and the maximum cohesive crack opening displacement is less than w_c. Equation (13) can be solved for two right-hand side vectors:

$$(\mathbf{K}-\mathbf{C})\mathbf{u}_1 = \mathbf{F}_v + \mathbf{F}_s, \tag{16a}$$

$$(\mathbf{K}-\mathbf{C})\mathbf{u}_2 = \mathbf{F}_u^+ + \mathbf{F}_u^-. \tag{16b}$$

At the fictitious crack tip, the stress vector can be written:

$$[\sigma_x, \sigma_y, \tau]^T = \lambda[\sigma_x, \sigma_y, \tau]_1^T + [\sigma_x, \sigma_y, \tau]_2^T \tag{17}$$

where λ is the external load multiplier.

In order to allow the crack propagation, the maximum principal stress, corresponding

to the stress vector (17), has to be equal to the tensile strength of the material:

$$\frac{\sigma_x+\sigma_y}{2}+\frac{1}{2}\sqrt{(\sigma_x-\sigma_y)^2+4\tau^2}=\sigma_u. \tag{18}$$

Substituting eqn (17) in eqn (18), it is possible to compute the external load multiplier λ. The angle between the x-axes and the normal to the principal plane, related to the principal stress (18), is given by:

$$\alpha=\frac{1}{2}\tan^{-1}\left[\frac{2\tau}{\sigma_x-\sigma_y}\right]. \tag{19}$$

The subsequent crack branch will occur in the principal plane denoted by eqn (19).

At the following steps the same procedure is repeated, without moving the real crack tip, until one of the following conditions is verified.

(1) The crack opening displacement at the real crack tip reaches its critical value w_c. In this case, the real crack tip moves and the cohesive crack surface S_c shrinks until the crack opening displacement at the real crack tip is less than w_c.
(2) Matrix $(\mathbf{K}-\mathbf{C})$ in eqn (16) becomes positive semi-definite. In this case, the stress vector at the fictitious crack tip can be written:

$$[\sigma_x,\sigma_y,\tau]^T=\mathbf{DBu}-\mathbf{D}\varepsilon_0+\sigma_0. \tag{20}$$

Equation (16) becomes:

$$(\mathbf{K}-\mathbf{C})\mathbf{u}=\lambda(\mathbf{F}_v+\mathbf{F}_s)+\mathbf{F}_u^+ +\mathbf{F}_u^-. \tag{21}$$

Substituting eqn (20) in eqn (18), a non-linear equation in $\mathbf{u}$ is obtained. The n equations (21) and eqn (18) represent a system of $n+1$ equations in $n+1$ unknowns $(\mathbf{u}, \lambda)$. Since eqn (18) is non-linear, the solution is computed using the Newton–Raphson method.

4. DISCUSSION

With reference to the experimental program described in Section 2, the maximum loading capacity P_{COHES} can be obtained according to the previous cohesive crack model. On the other hand, the maximum load P_{LEFM} of brittle fracture can be derived from the

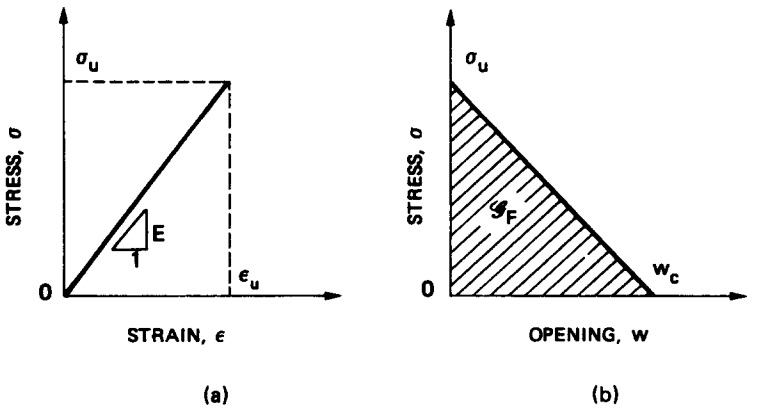

Fig. 5. Stress vs strain and stress vs crack opening displacement constitutive laws.

application of the Maximum Circumferential Stress Criterion (Erdogan and Sih, 1963):

$$\frac{d\sigma_\theta}{d\theta} = 0, \quad \sigma_\theta\sqrt{2\pi r} = K_{IC} = \sqrt{\mathscr{G}_F E}. \tag{22}$$

Stress intensification is produced in both the crack tip regions and the stress intensity factors for Mode I and Mode II can be expressed respectively as:

$$K_I = \frac{P}{tb^{1/2}} f_I\left(\frac{l}{b}, \frac{a}{b}, \frac{c}{b}\right), \tag{23a}$$

$$K_{II} = \frac{P}{tb^{1/2}} f_{II}\left(\frac{l}{b}, \frac{a}{b}, \frac{c}{b}\right), \tag{23b}$$

f_I and f_{II} being the shape functions.

The angle θ_0 of crack branching is provided by the following equation:

$$f_I \sin\theta_0 + f_{II}(3\cos\theta_0 - 1) = 0, \tag{24}$$

whereas the mixed mode crack instability is predicted by the condition:

$$P_{LEFM} \cos\frac{\theta_0}{2}\left[f_I \cos^2\frac{\theta_0}{2} - \frac{3}{2} f_{II} \sin\theta_0\right] = tb^{1/2} K_{IC}. \tag{25}$$

The values of the ratio P_{COHES}/P_{LEFM} are represented in Fig. 6 against the dimensionless size $1/s_E$. A transition is evident towards LEFM by increasing the size-scale of the structure. For the brittler geometry, $c/b = 0.4$, the transition appears to be faster, and already for $b\sigma_u/\mathscr{G}_F = 2 \times 10^4$ or $s_E = 5 \times 10^{-5}$, the asymptotical LEFM condition is achieved. In this case, the size of the cohesive zone is negligible with respect to the size of the zone where the $r^{-1/2}$ LEFM stress singularity is dominant. For the more ductile geometry, $c/b = 0.8$, the experimental results present the same trend as that of the numerical ones.

For $c/b = 0.8$, the total load versus loading point deflection diagrams are plotted in Fig. 7a, b, for the cases $b = 5$ and 20 cm respectively. The mixed mode cohesive crack model describes both the experimental curves satisfactorily. The size $b = 20$ cm (Fig. 7b) produces snap-back instability in the experimental as well as in the numerical curve. The area enclosed

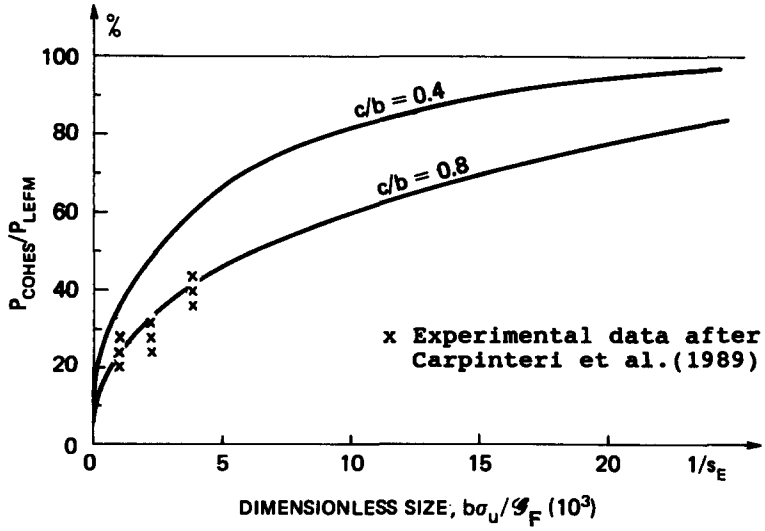

Fig. 6. Size-scale transition towards mixed mode brittle fracture (LEFM instability).

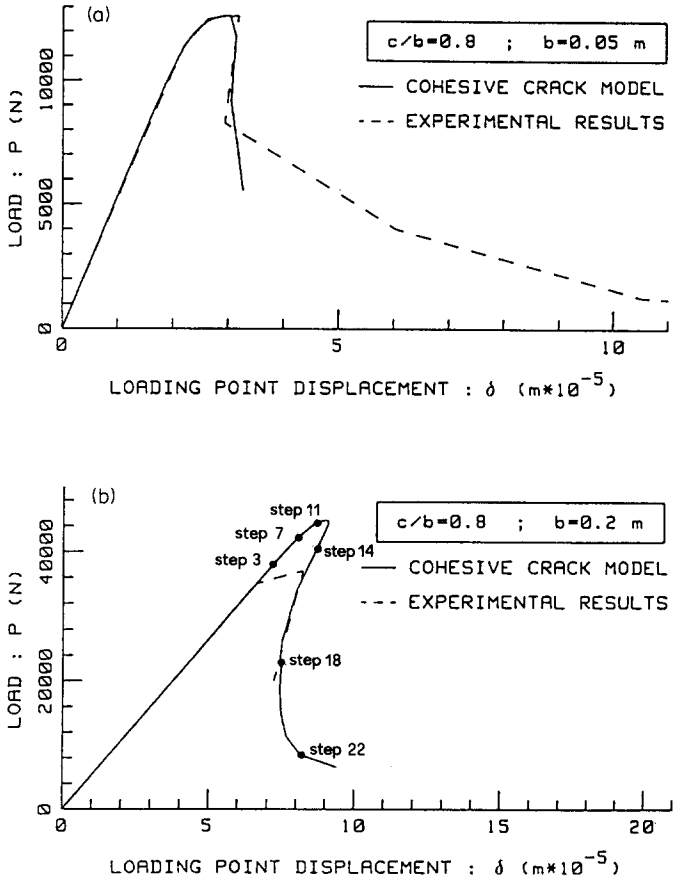

Fig. 7. Experimental load vs deflection curves and numerical cohesive crack simulation for $c/b = 0.8$. (a) $b = 5$ cm; (b) $b = 20$ cm.

between the numerical curve and deflection axis is approximately equal to the product of the Mode I fracture energy $\mathcal{G}_F$ and the total fracture area, and represents the amount of energy dissipated in the localized fracture zone. The amount of energy dissipated by punching at the supports was deliberately neglected, assuming ascending elastic branches consistent with the elastic modulus of the material.

It is remarkable that the application of the usual Mode I fracture energy $\mathcal{G}_F$ only was able to provide consistent results. It was unnecessary to introduce additional fracture toughness parameters, like, for example, the Mode II fracture energy $\mathcal{G}_F^{II}$ (Rots and de Borst, 1987; Bažant and Pfeiffer, 1986). As a matter of fact, the mixed mode fracture energy has a value approximately equal to Mode I fracture energy $\mathcal{G}_F$, each elementary crack growth step being produced by a Mode I (or opening) mechanism along the curvilinear trajectory.

The sequence of the finite element meshes utilized for the case $b = 20$ cm, $c/b = 0.8$ is reported in Fig. 8. The trajectory of the finite element rosette reproduces the experimental fracture trajectory accurately.

According to the cohesive model, the length of the process zone is not a constant. On the contrary, it depends on the mechanical properties of the body at each step of the crack growth. In the present example the real crack (complete disconnection) starts propagating only at the thirteenth step, when the fictitious crack (cohesive interaction) is beyond one half of the beam depth. On the other hand, at the twenty-second step, both fictitious and real crack tip are close to the upper beam edge. The single steps are also indicated in the diagram of Fig. 7b. For the same case, the subsequent deformed configurations are reported in Fig. 9.

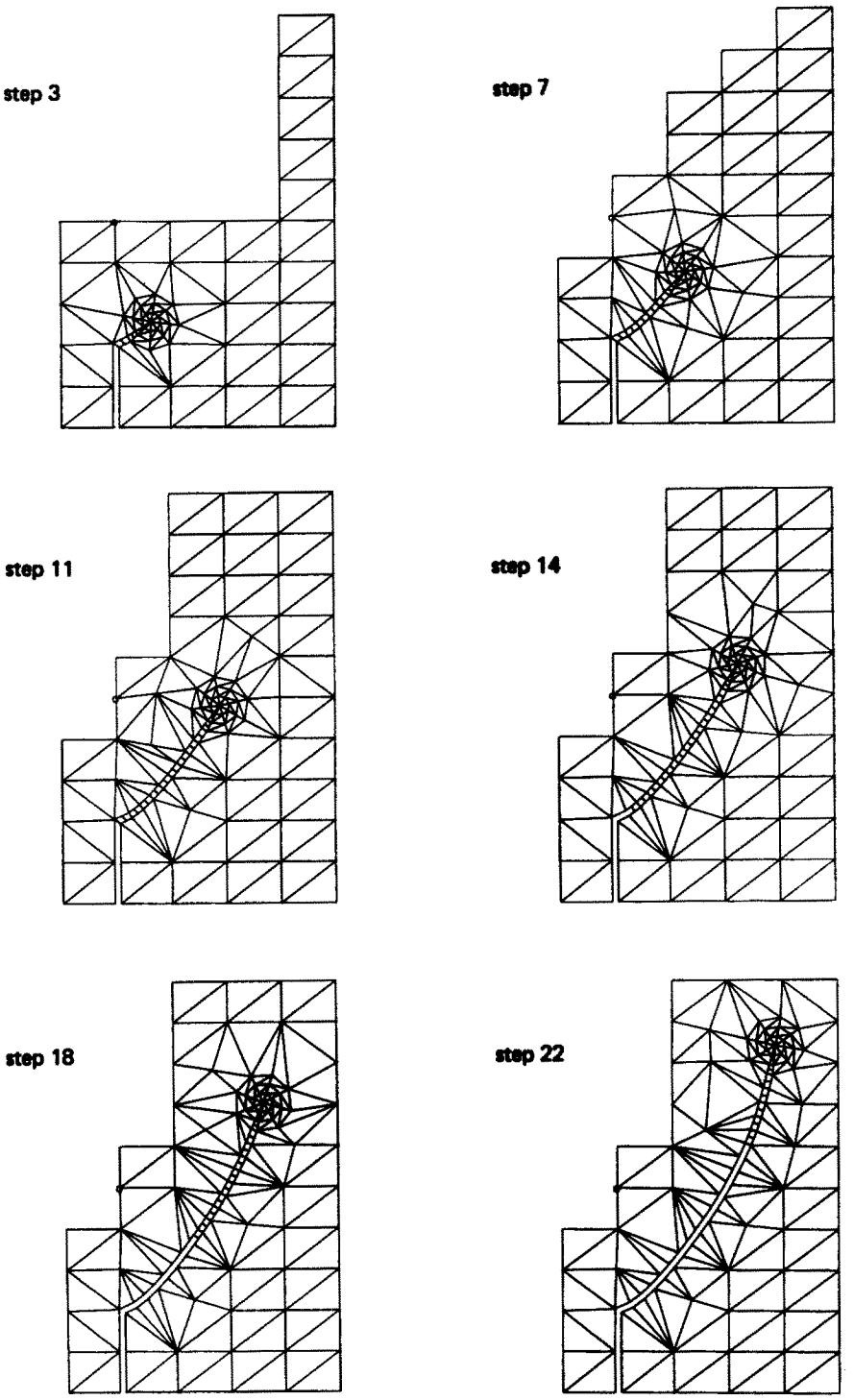

Fig. 8. Finite element remeshing for $c/b = 0.8$, $b = 20$ cm.

A real mixed mode crack propagation developed only in the specimens with the ratios $c/b = 0.4$ and 0.8, whereas for $c/b = 1.2$ a bending failure at the supports prevailed. For $b = 5$, 10, 20 cm and $c/b = 0.4$, 0.8, all the experimental crack trajectories are reported in Fig. 10 (for $b = 5$, 10 cm it was preferred to group all the trajectories on one side). The statistical dispersion appears to be independent of specimen geometry and size, and to be of the same order of magnitude as that of the aggregates. The trajectories simulated numerically (thick dashed lines) are in good agreement with the experimental ones.

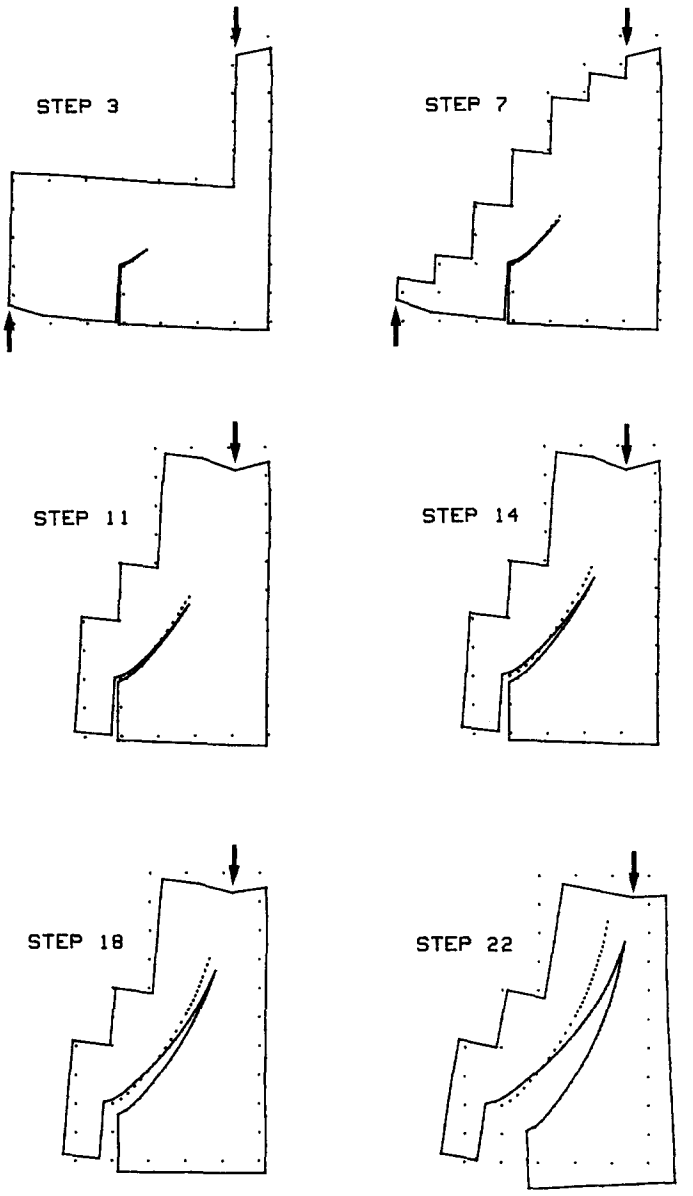

Fig. 9. Subsequent deformed configurations for $c/b = 0.8$, $b = 20$ cm. Displacement magnification factor: 300.

5. CONCLUSIONS

(1) The brittleness in the experiments is controlled by imposing a constant crack mouth sliding displacement rate (monotonic increasing function of time).

(2) The brittleness in the numerical simulations is controlled through the crack length, which is certainly a monotonic increasing function during the irreversible fracture process.

(3) The mixed mode fracture energy is found to be of the same order of magnitude as the Mode I fracture energy $\mathscr{G}_F$, each elementary crack growth step being produced by a Mode I (or opening) mechanism along the curvilinear trajectory. This is particularly true for the larger specimens, where energy dissipation due to friction and interlocking is negligible if compared with the energy dissipated by separation.

(4) The trajectories simulated numerically are in good agreement with the experimental ones. The latter show a statistical dispersion which is independent of specimen size and of the same order of magnitude as that of the aggregates.

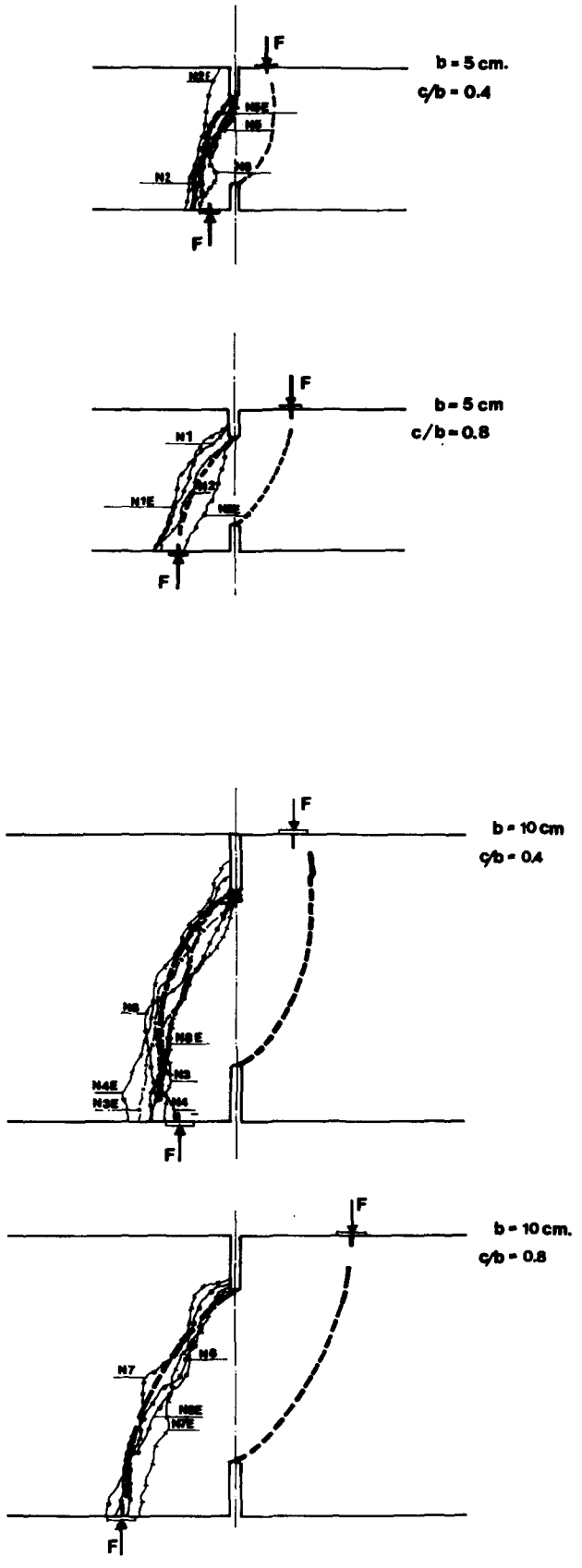

Fig. 10. Experimental and numerical crack trajectories for $b = 5$, 10, 20 cm and $c/b = 0.4$, 0.8.

(*Continued overleaf.*)

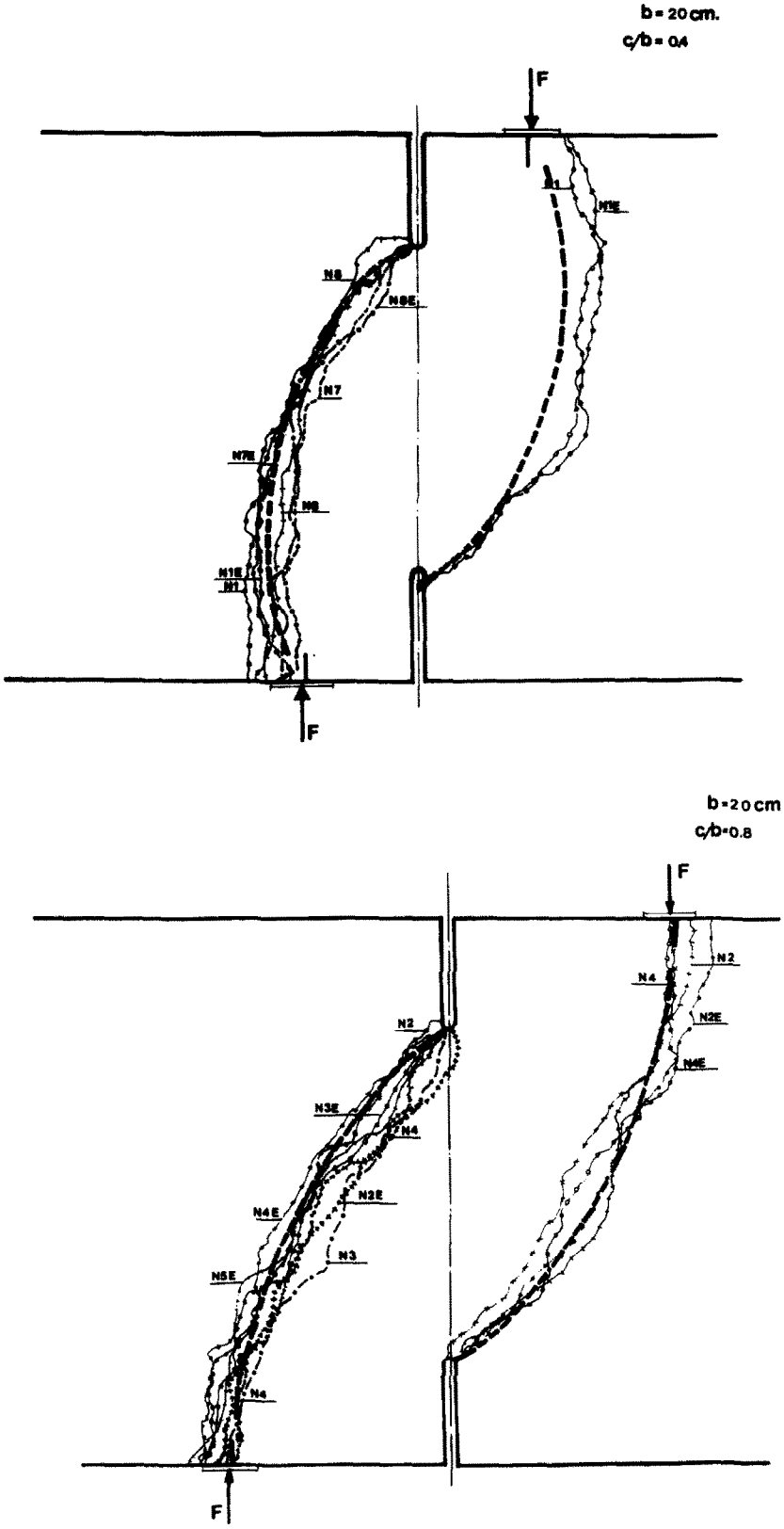

Fig. 10. (*continued*).

Acknowledgements—The present research was financially supported by the Department of Public Education (M.P.I.) and by the National Research Council (C.N.R.).

REFERENCES

Barenblatt, G. I. (1959). The formation of equilibrium cracks during brittle fracture: general ideas and hypotheses. Axially-symmetric cracks. *J. Appl. Math. Mech.* **23,** 622–636.

Bazănt, Z. P. and Pfeiffer, P. A. (1986). Shear fracture tests of concrete. *Mater. Struct.* **19,** 111–121.

Bilby, B. A., Cottrell, A. H. and Swinden, K. H. (1963). The spread of plastic yield from a notch. *Proc. R. Soc.* **A272,** 304–314.

Carpinteri, A. (1984). Interpretation of the Griffith instability as a bifurcation of the global equilibrium. In *NATO Advanced Research Workshop on Application of Fracture Mechanics to Cementitious Composites* (Edited by S. P. Shah), pp. 284–316, Evanston, IL, 4–7 September 1984. Martinus Nijhoff, Dordrecht (1985).

Carpinteri, A. (1989a). Decrease of apparent tensile and bending strength with specimen size: two different explanations based on fracture mechanics. *Int. J. Solids Structures* **25,** 407–429.

Carpinteri, A. (1989b). Post-peak and post-bifurcation analysis of cohesive crack propagation. *Engng Fracture Mech.* **32,** 265–278.

Carpinteri, A. and Colombo, G. (1989). Numerical analysis of catastrophic softening behaviour (snap-back instability). *Comput. Struct.* **31,** 607–636.

Carpinteri, A. and Fanelli, M. (1987). Numerical analysis of the catastrophical softening behaviour in brittle structures. *Fourth International Conference on Numerical Methods in Fracture Mechanics*, pp. 369–386, San Antonio, TX, 23–27 March 1987. Pineridge Press, Swansea.

Carpinteri, A. and Valente, S. (1988). Numerical modelling of mixed mode cohesive crack propagation. In *International Conference on Computational Engineering Science* (Edited by S. N. Atluri and G. Yagawa), pp. 12–VI, Atlanta, GA, April 10–14, 1988. Springer, New York.

Carpinteri, A., Valente, S. and Bocca, P. (1989). Mixed mode cohesive crack propagation. *Seventh International Conference on Fracture* (ICF7), pp. 2243–2257, Houston, TX, 20–24 March 1989. Pergamon Press, Oxford.

Dugdale, D. S. (1960). Yielding of steel sheets containing slits. *J. Mech. Phys. Solids* **8,** 100–104.

Erdogan, F. and Sih, G. C. (1963). On the crack extension in plates under plane loading and transverse shear. *J. Basic Engng* **85,** 519–527.

Hillerborg, A., Modeer, M. and Petersson, P. E. (1976). Analysis of crack formation and crack growth in concrete by means of fracture mechanics and finite elements. *Cement Concrete Res.* **6,** 773–782.

Rice, J. R. (1968). A path independent integral and the approximate analysis of strain concentration by notches and cracks. *J. Appl. Mech.* **35,** 379–386.

RILEM Recommendation (1985). Determination of the fracture energy of mortar and concrete by means of three point bend tests on notched beams. *Mater. Struct.* **18,** 287–290.

Rots, J. G. and de Borst, R. (1987). Analysis of mixed mode fracture in concrete. *J. Engng Mech.* **113,** 1739–1758.

Wawrzynek, P. A. and Ingraffea, A. R. (1987). Interactive finite element analysis of fracture processes: an integrated approach. *Theor. Appl. Fracture Mech.* **8,** 137–150.

Willis, J. R. (1967). A comparison of the fracture criteria of Griffith and Barenblatt. *J. Mech. Phys. Solids* **15,** 151–162.

Wnuk, M. P. (1974). Quasi-static extension of a tensile crack contained in a viscoelastic–plastic solid. *J. Appl. Mech.* **41,** 234–242.